NASA MEMO 4-14-59L

# NASA

# MEMORANDUM

## FLUTTER INVESTIGATION AT A MACH NUMBER OF 7.2 OF MODELS OF THE HORIZONTAL- AND VERTICAL-TAIL SURFACES OF THE X-15 AIRPLANE

By Frederick W. Gibson and John S. Mixson

Langley Research Center
Langley Field, Va.





NATIONAL AERONAUTICS AND SPACE ADMINISTRATION

WASHINGTON

May 1959

[redacted]

NATIONAL AERONAUTICS AND SPACE ADMINISTRATION

MEMORANDUM 4-14-59L



# FLUTTER INVESTIGATION AT A MACH NUMBER OF 7.2 OF MODELS OF THE HORIZONTAL- AND VERTICAL-TAIL SURFACES OF THE X-15 AIRPLANE

By Frederick W. Gibson and John S. Mixson

## SUMMARY

The results of a flutter investigation of 1/12-scale models of the all-movable horizontal and vertical tails of the X-15 airplane are presented. Two semispan models of the horizontal tail and one model of the vertical tail were tested at a Mach number of 7.2 in the 8-inch-diameter test section of the Langley hypersonic aeroelasticity tunnel. One horizontal-tail model was tested at an angle of attack of $0^\circ$ and fluttered. The other horizontal-tail model was tested at approximately an angle of attack of $10^\circ$ and failed statically before flutter was obtained. The vertical-tail model was tested at an angle of attack of $0^\circ$ and fluttered.

The dynamic pressures at flutter of the horizontal- and vertical-tail models were 2,500 pounds per square foot and 1,650 pounds per square foot, respectively, corresponding to full-scale values of 13,500 pounds per square foot and 8,900 pounds per square foot. Since the full-scale airplane is not expected to be subjected to a dynamic pressure in excess of 2,500 pounds per square foot, a large factor of safety is indicated. Calculations of the flutter speed of the two models that fluttered in the tests were made by using the aerodynamic forces derived from piston theory. The experimental and theoretical results showed good agreement.

## INTRODUCTION

The widespread use of all-movable control surfaces on high-performance aircraft and missiles has lead to increased interest in the flutter characteristics of such configurations. References 1 and 2 report results of a

*Title, Unclassified.

[redacted]

research program in which rectangular-plan-form, all-movable controls were tested at Mach numbers of 6.86 and 7.2. Reference 3 reports the results of tests for possible flutter of a dynamically and elastically scaled model of the X-15 horizontal all-movable tail surfaces at a Mach number of 6.86.

As an extension of the program of flutter testing of all-movable control surfaces, tests were made at a Mach number of 7.2 in the Langley hypersonic aeroelasticity tunnel on two semispan, 1/12-scale models of the horizontal-tail surface and one 1/12-scale semispan model of the upper vertical-tail surface of the X-15 airplane.

The experimental flutter results and the results of theoretical flutter calculations are presented. The calculations were made by using aerodynamic forces derived from second-order piston theory (ref. 4) and experimentally determined mode shapes and frequencies.

## SYMBOLS

| | |
|---|---|
| $a$ | velocity of sound, ft/sec |
| $b$ | one-half chord, ft |
| $b_r$ | one-half root chord, ft |
| $f$ | frequency, cps |
| $k$ | reduced frequency, $b\omega/V$ |
| $l$ | general dimension of length |
| $m$ | mass of control surface, slugs |
| $M$ | Mach number |
| $q$ | dynamic pressure, lb/sq ft |
| $V$ | velocity, ft/sec |
| $\alpha$ | angle of attack, deg |
| $\mu$ | mass ratio, $\dfrac{m}{\pi\rho \int_0^l b^2 dl}$ |

[redacted]

$\rho$ density, slugs/cu ft

$\omega$ circular frequency, radians/sec

EI bending stiffness, lb-ft$^2$

Subscripts:

1,2,3 indicate natural vibration modes in order of ascending frequency

F indicates flutter condition

S indicates model values

A indicates full-scale airplane values

## MODEL DESCRIPTION

Three models were tested, one vertical-tail and two horizontal-tail surfaces designated V-1, H-1, and H-2, respectively.

### Geometry and Construction

The plan forms and dimensions of the horizontal- and vertical-tail surfaces are shown in figures 1 and 2, respectively. The model of the horizontal tail was 1/12 scale with an aspect ratio of approximately 2.5, a taper ratio of 0.305, and a sweep angle of 45° at the quarter-chord line. The airfoil was an NACA 66A005 section modified so that it was 1 percent thick at the trailing edge with a straight-line fairing to the point of tangency. The construction consisted of an aluminum box spar and aluminum ribs, the remainder being balsa with lead masses distributed as shown in figure 3. The axis of rotation was at approximately 56 percent of the root chord and the spindle was restrained by flex springs to give the desired natural frequencies. The model of the vertical tail was 1/12 scale. The leading edge was swept back $28\frac{1}{2}^\circ$ and the trailing edge was unswept. The airfoil was a 10° wedge with a leading-edge radius of approximately 0.5-percent chord and the trailing-edge thickness was about 19-percent chord. The construction of this model is illustrated in figure 4 and consisted of a spar and rib covered with balsa and an aluminum skin over approximately 50 percent of the chord. One lead mass was placed at the leading-edge tip juncture. The inboard one-third of the model was fixed with the outboard two-thirds movable about the center of rotation

[redacted]

which was located at approximately 36 percent of the root chord on the spindle. The spindle was restrained by flex springs to give the desired natural frequencies.

The models were designed to be true Mach number dynamically scaled models representing the tail surfaces of the X-15 airplane flying at a Mach number of 7.0 at an altitude of 40,000 feet. This combination of Mach number and altitude represents extreme conditions to which the airplane is not expected to be subjected in its flight regime but which nevertheless were considered necessary because of the restrictions imposed by available tunnel capabilities. From these considerations the following scale factors were determined:

Selected values:

$$\frac{l_S}{l_A} = \frac{1}{12}$$

$$\frac{a_S}{a_A} = 0.774$$

$$\frac{\rho_S}{\rho_A} = 0.309$$

Computed values:

$$\frac{m_S}{m_A} = \frac{\rho_S}{\rho_A}\left(\frac{l_S}{l_A}\right)^3 = 0.1787 \times 10^{-3}$$

$$\frac{\omega_S}{\omega_A} = \frac{a_S}{a_A}\left(\frac{l_S}{l_A}\right)^{-1} = 9.2975$$

$$\frac{EI_S}{EI_A} = \frac{\rho_S}{\rho_A}\left(\frac{a_S}{a_A}\right)^2\left(\frac{l_S}{l_A}\right)^4 = 0.8939 \times 10^{-5}$$

$$\frac{q_S}{q_A} = \frac{\rho_S}{\rho_A}\left(\frac{a_S}{a_A}\right)^2 = 0.1851$$

where S and A represent the model and full-scale values, respectively.

The stiffnesses simulated by the models were those of the full-scale airplane tail surfaces at maximum temperature with skin buckled, the rotational stiffness being 130 percent of nominal. However, only the total stiffnesses of the full-scale tail surfaces were simulated, no attempt being made to duplicate local values.

## Vibration Characteristics

The dynamic characteristics of the models were determined in the laboratory by using the arrangement shown in figure 5. The model was mounted on a backstop in a manner simulating the support system used for the tunnel tests. An air shaker (described in ref. 5) was placed under the wing and the frequency varied until resonance in one of the various modes occurred. The mode shapes of model H-1 were obtained by the photographic technique described in reference 6. A typical photograph of the model vibrating in a resonant frequency is reproduced in figure 5. Sketches of the mode shapes and of the node lines of the first three natural frequencies of model H-1 are shown in figure 6. The normalized modes of model H-1 are presented in table I. In order to avoid the risk of damage to the model V-1, it was not driven at large enough amplitudes to measure the mode shapes by the photographic technique. Therefore, the mode shapes for the first two natural frequencies were estimated from the node lines which were observed by sprinkling sand on the vibrating model. A sketch of these node lines is presented in figure 7.

## TUNNEL DESCRIPTION

The tests were run in the 8-inch-diameter test section of the Langley hypersonic aeroelasticity tunnel which uses helium as the testing medium. Some of the characteristics of helium as a flutter testing medium are discussed in reference 2. This tunnel is of the blowdown type and the test section used had a Mach number of 7.2 and a maximum dynamic pressure of about 5,000 pounds per square foot. Figure 8 shows the Mach number distribution across the test section at several stations along the stream direction.

## INSTRUMENTATION

A recording oscillograph was used during each test to obtain continuous records of the output of strain gages oriented on the model spindle about two different axes to indicate, primarily, bending and

pitching motions. Simultaneously recorded were the outputs of a thermocouple and a pressure cell from which tunnel stagnation temperature and pressure could be determined. Motion pictures at a speed of approximately 800 frames per second were obtained of the flutter of model V-1.

## TEST PROCEDURE

The models were mounted on a reflection plane in the test section as shown in figure 9 which also shows the spacer block used to extend the model and the reflection plane out of the boundary layer. Models H-1 and V-1 were tested at an angle of attack of $0^\circ$ and model H-2 was tested at approximately $10^\circ$.

At the start of the tests, the tunnel was opened to a downstream vacuum of approximately 1/2 inch of mercury absolute. During the tests, the stagnation pressure was increased at a moderate rate until the model either fluttered or failed statically. When this procedure was used, the tests were of approximately 15 seconds duration.

## RESULTS AND DISCUSSION

A summary of the test results is presented in table II, which lists the mass of the models, the natural frequencies, test-section density, speed of sound, and dynamic pressure at the start of flutter of models H-1 and V-1 and at the point of static failure of model H-2. Also given are the flutter frequencies of the two models that fluttered. A motion-picture sequence showing the flutter of model V-1 is presented in figure 10 and the corresponding oscillograph record is shown in figure 11. The photographs and record both show the buildup of flutter from small-amplitude oscillations to large destructive amplitudes.

Figures 12 and 13 show comparisons of the experimental and calculated flutter parameters $\frac{b_r \omega_2}{a}\sqrt{\mu}$ for models H-1 and V-1, respectively, which were tested at an angle of attack of $0^\circ$. These calculations were made by following the procedure of reference 7 by using the aerodynamic forces derived from second-order piston theory, the experimentally determined natural frequencies and mode shapes of the first three modes of model H-1, and the experimentally determined frequencies and estimated mode shapes of the first two modes of model V-1. Thickness effects were included. The results show excellent agreement between the theory and experiment for model H-1 for which the actual measured mode shapes were used in the theoretical calculations. In the case of model V-1, the experimental and theoretical results were in somewhat poorer agreement. Included in

figure 12 is the experimental value of the parameter $\frac{b_r\omega_2}{a}\sqrt{\mu}$ for model H-2 at the point where the model failed statically because of the loads imposed by the angle of attack. Also included in figure 12 is a theoretical flutter boundary for an angle of attack of 10° which was calculated by North American Aviation Corporation by using aerodynamic forces derived from third-order piston theory. The section of the curve that is solid is believed to be within the limitation of piston theory. This limitation is fixed by the premise that the ratio of the component of velocity normal to the airfoil to the local speed of sound be less than unity. The theoretical calculations of figure 12 indicate enlargement of the flutter region due to increased angle of attack. Model H-2 failed statically at an angle of attack of 10° just before the theoretical flutter region was reached.

The dynamic pressure at flutter of models H-1 and V-1, as given in table II, were 2,500 and 1,650 pounds per square foot, respectively, corresponding to full-scale values of 13,500 pounds per square foot and 8,900 pounds per square foot. Since the full-scale airplane is not expected to be subjected to a dynamic pressure in excess of 2,500 pounds per square foot, a large factor of safety appears to be indicated. However, it must be pointed out that in scaling the models, only the total stiffnesses of the full-scale airplane tail surfaces as individual cantilevers were simulated. The effects of local stiffnesses and possible reactions between the horizontal- and vertical-tail surfaces and between the body motions and the tail surfaces were not considered.

## CONCLUDING REMARKS

Flutter tests have been conducted on dynamically and elastically scaled models of the horizontal- and vertical-tail surfaces of the X-15 airplane. The tests were run at a Mach number of 7.2 in an 8-inch-diameter test section of the Langley hypersonic aeroelasticity tunnel, which uses helium as a testing medium. One horizontal-tail model fluttered at a dynamic pressure of 2,500 pounds per square foot at an angle of attack of 0° and an approximately identical model failed statically before flutter was obtained when tested at an angle of attack of 10°. The vertical-tail model fluttered at a dynamic pressure of 1,650 pounds per square foot at an angle of attack of 0°. The corresponding full-scale values of dynamic pressure for the two models that fluttered are 13,500 pounds per square foot and 8,900 pounds per square foot, respectively. Since the full-scale airplane is not expected to be subjected to a dynamic pressure in excess of 2,500 pounds per square foot, a large factor of safety appears to be indicated. However, for these tests, only the total stiffnesses of the full-scale airplane tail surfaces as individual cantilevers were simulated. The effects of local stiffnesses and

possible reactions between the horizontal- and vertical-tail surfaces and between the body motions and the tail surfaces were not considered.

Good agreement was obtained between the experimental results and theoretical calculations made by using aerodynamic forces derived from second-order piston theory and experimentally determined mode shapes and frequencies.

Langley Research Center,
National Aeronautics and Space Administration,
Langley Field, Va., January 22, 1959.

## REFERENCES

1. Runyan, Harry L., and Morgan, Homer G.: Flutter at Very High Speeds. NACA RM L57D16a, 1957.

2. Morgan, Homer G., and Miller, Robert W.: Flutter Tests of Some Simple Models at a Mach Number of 7.2 in Helium Flow. NASA MEMO 4-8-59L, 1959.

3. Lauten, William T., Jr., Levey, Gilbert M., and Armstrong, William O.: Investigation of an All-Movable Control Surface at a Mach number of 6.86 for Possible Flutter. NACA RM L58B27, 1958.

4. Ashley, Holt, and Zartarian, Garabed: Piston Theory - A New Aerodynamic Tool for the Aeroelastician. Jour. Aero. Sci., vol. 23, no. 12, Dec. 1956, pp. 1109-1118.

5. Herr, Robert W.: A Wide-Frequency-Range Air-Jet Shaker. NACA TN 4060, 1957.

6. Herr, Robert W.: Preliminary Experimental Investigation of Flutter Characteristics of M and W Wings. NACA RM L51E31, 1951.

7. Morgan, Homer G., Huckel, Vera, and Runyan, Harry L.: Procedure for Calculating Flutter at High Supersonic Speed Including Camber Deflections, and Comparison With Experimental Results. NACA TN 4335, 1958.

TABLE I.- NORMALIZED VIBRATION MODES OF HORIZONTAL CONTROL SURFACE, H-1

| Fraction span | Fraction chord | | | | |
|---|---|---|---|---|---|
| | 0 | 0.25 | 0.50 | 0.75 | 1.00 |
| First mode | | | | | |
| 0 | 0.15 | 0.15 | 0 | -0.14 | -0.24 |
| .2 | .12 | .09 | -.07 | -.17 | -.28 |
| .4 | .06 | -.09 | -.16 | -.26 | -.38 |
| .6 | -.14 | -.22 | -.34 | -.53 | -.55 |
| .8 | -.35 | -.45 | -.54 | -.65 | -.80 |
| 1.0 | -.66 | -.73 | -.80 | -.87 | -1.00 |
| Second mode | | | | | |
| 0 | 0.98 | 0.50 | -0.03 | -0.55 | -0.84 |
| .2 | .72 | .37 | -.15 | -.60 | -1.00 |
| .4 | .53 | .21 | -.22 | -.56 | -.98 |
| .6 | .38 | .15 | -.15 | -.45 | -.61 |
| .8 | .35 | .14 | .14 | -.12 | -.16 |
| 1.0 | .77 | .62 | .65 | .69 | .77 |
| Third mode | | | | | |
| 0 | 0.50 | 0.23 | 0.16 | 0.07 | 0.32 |
| .2 | .46 | .35 | .25 | .26 | .35 |
| .4 | .51 | .47 | .36 | .31 | .20 |
| .6 | .67 | .60 | .38 | .18 | -.11 |
| .8 | .78 | .55 | .26 | -.20 | -.52 |
| 1.0 | .65 | .19 | -.53 | -.78 | -1.00 |

[redacted]



TABLE II.- EXPERIMENTAL FLUTTER DATA

[Horizontal-tail model, H-1, and vertical-tail model, V-1, fluttered. Horizontal-tail model, H-2, failed statically.]

| Model | m | $f_1$ | $f_2$ | $f_3$ | $f_F$ | q | $\rho$ | a | $\alpha$ |
|---|---|---|---|---|---|---|---|---|---|
| H-1 | 0.00185 | 96 | 294 | 381 | 185 | 2,500 | 0.000131 | 858.8 | 0 |
| H-2 | .00180 | 96.6 | 276 | 372 | --- | 1,450 | .0000874 | 801 | 11 |
| V-1 | .001096 | 120 | 280 | | 180 | 1,650 | .0000925 | 828.2 | 0 |

[redacted]

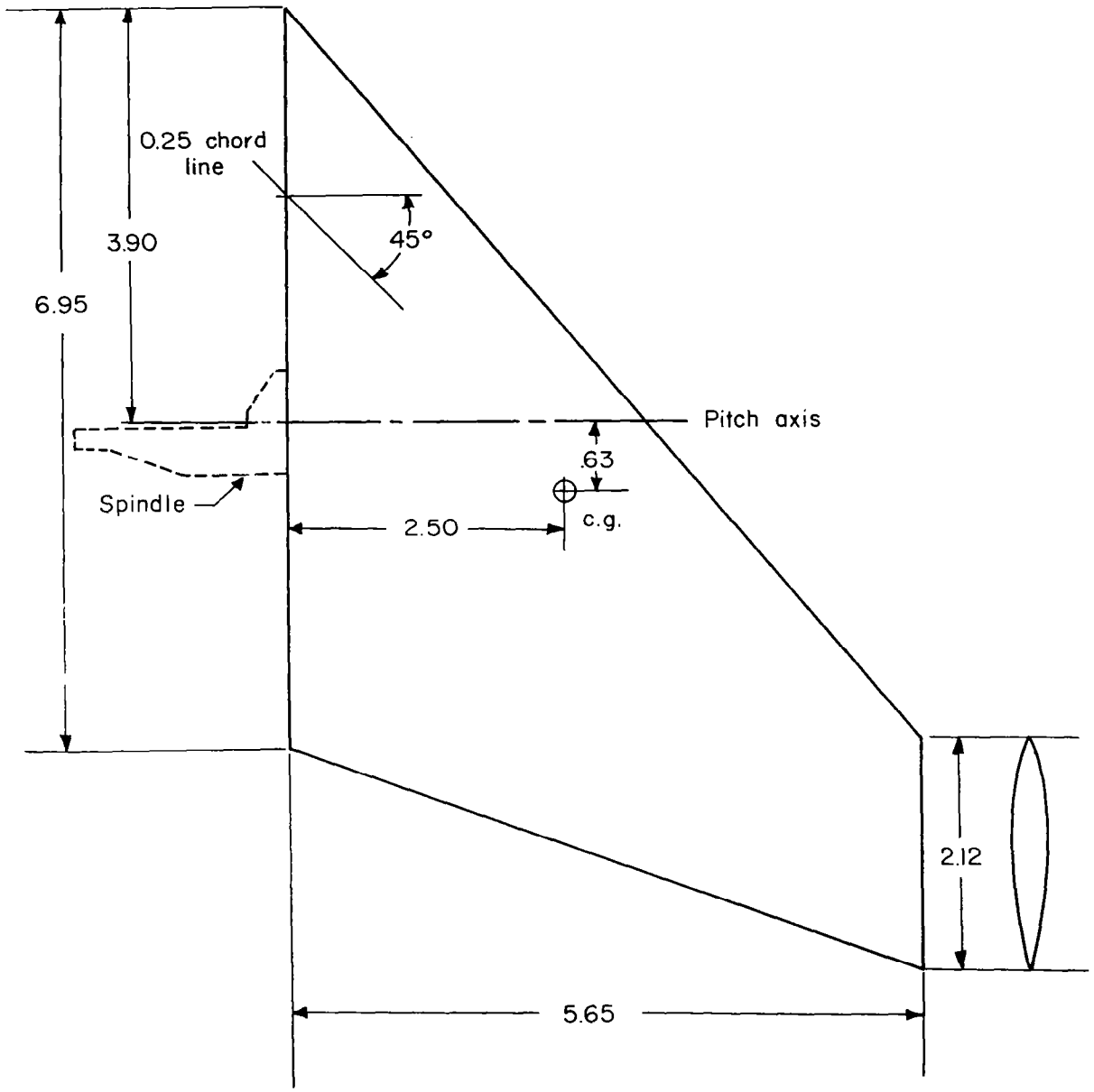


Figure 1.- Sketch of horizontal-tail models H-1 and H-2. All dimensions are in inches.

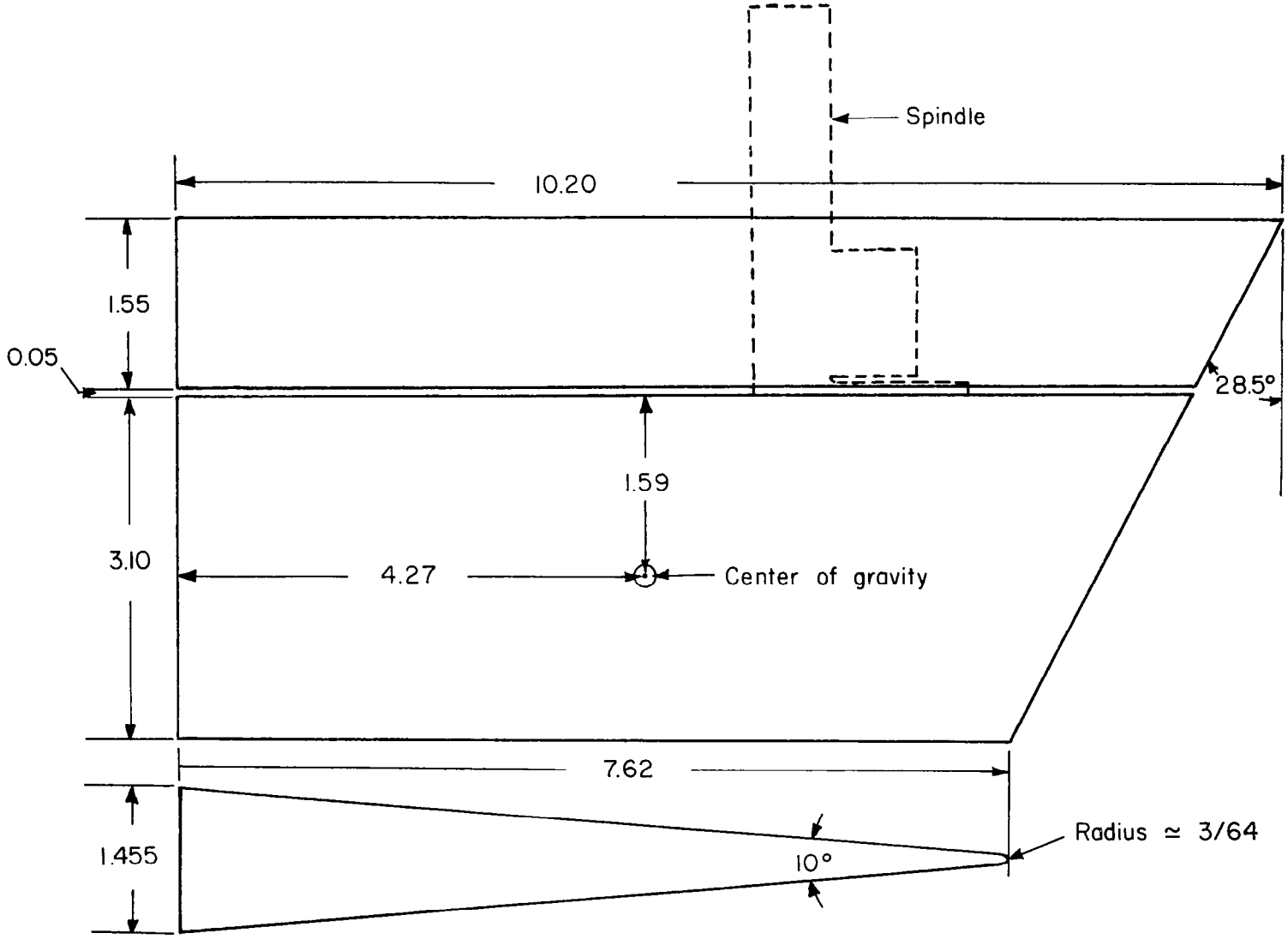


Figure 2.- Sketch of vertical-tail model V-1.

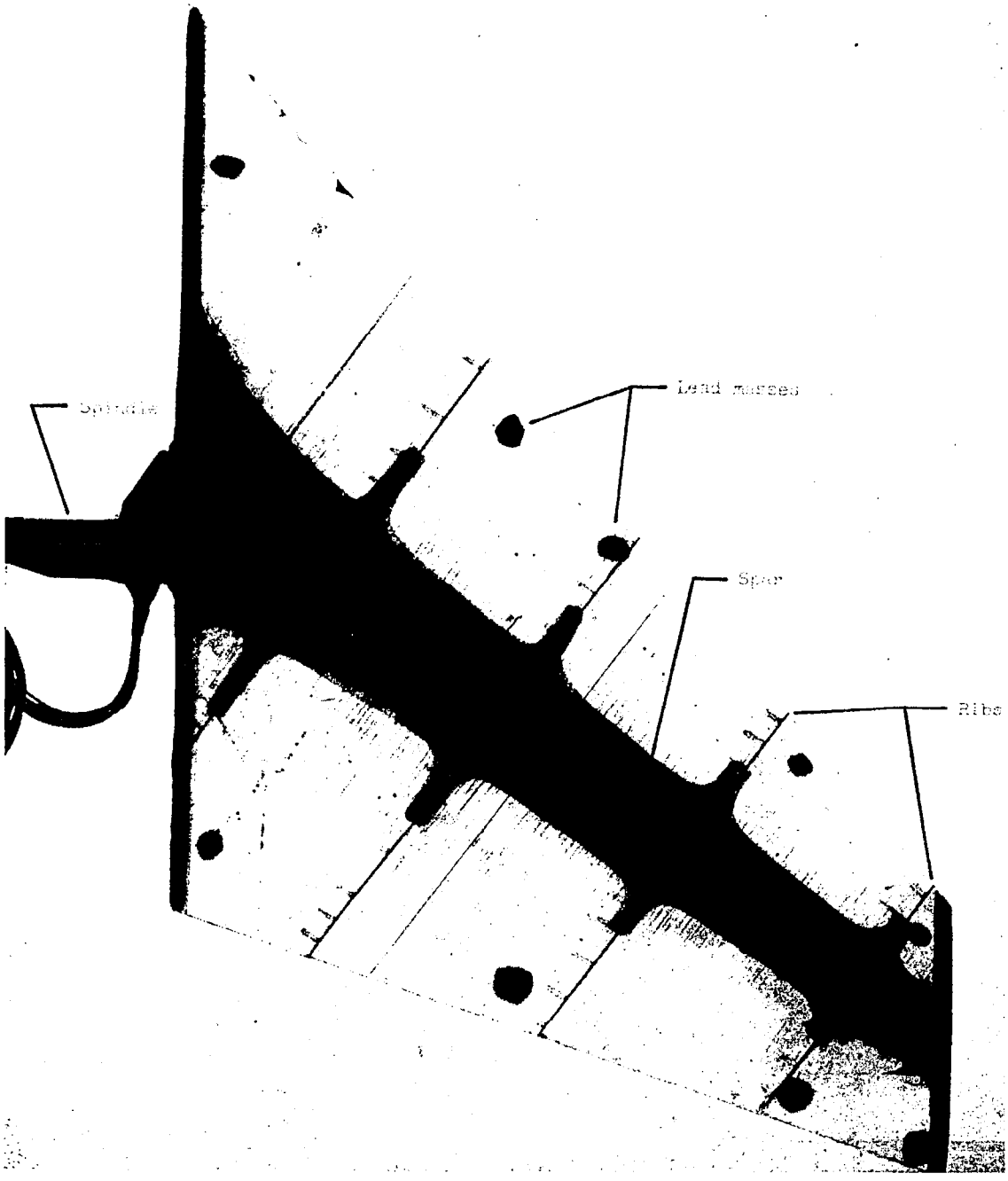


Figure 3.- X-ray photograph of horizontal-tail model H-1. L-59-195

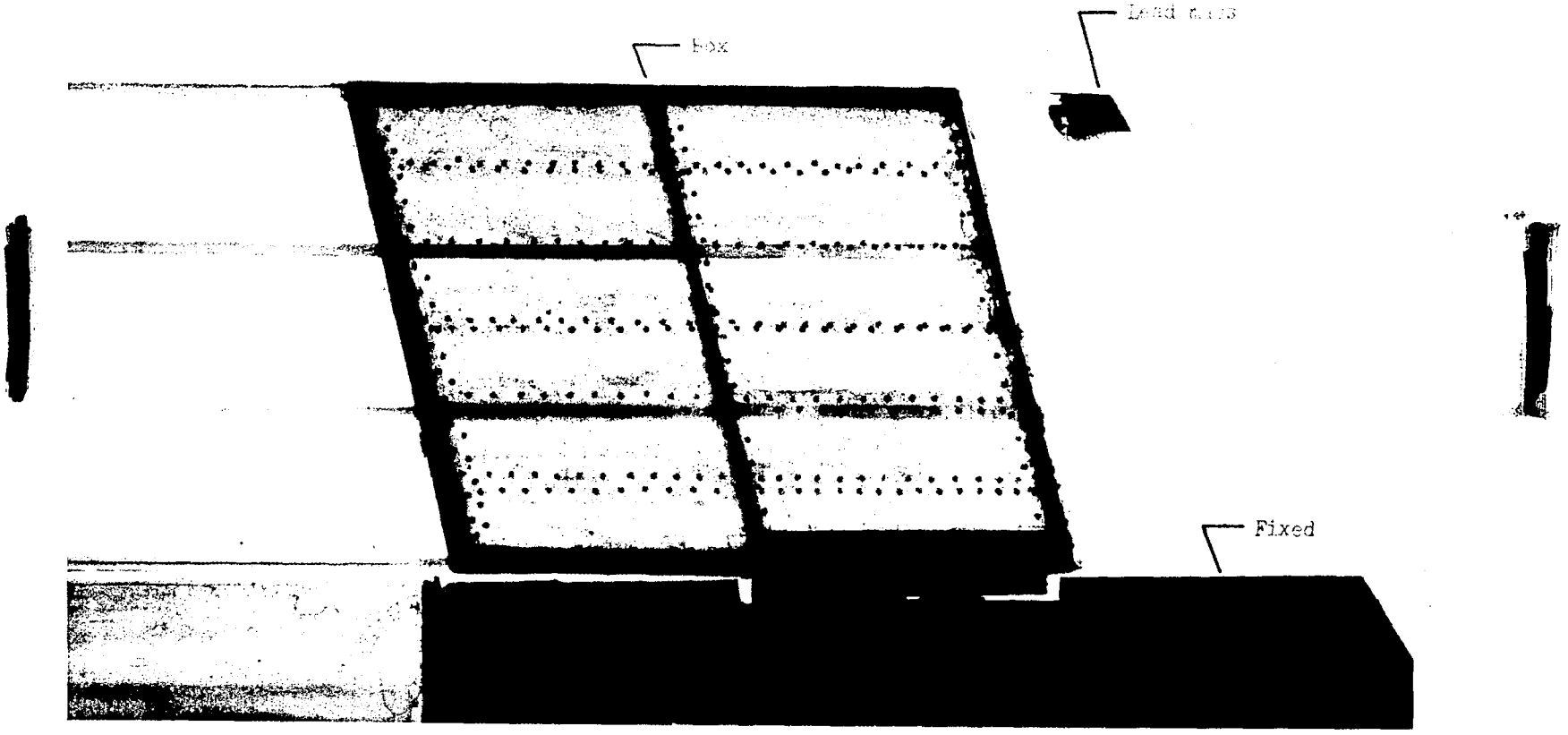


Figure 4.- X-ray photograph of vertical-tail model V-1. L-59-196

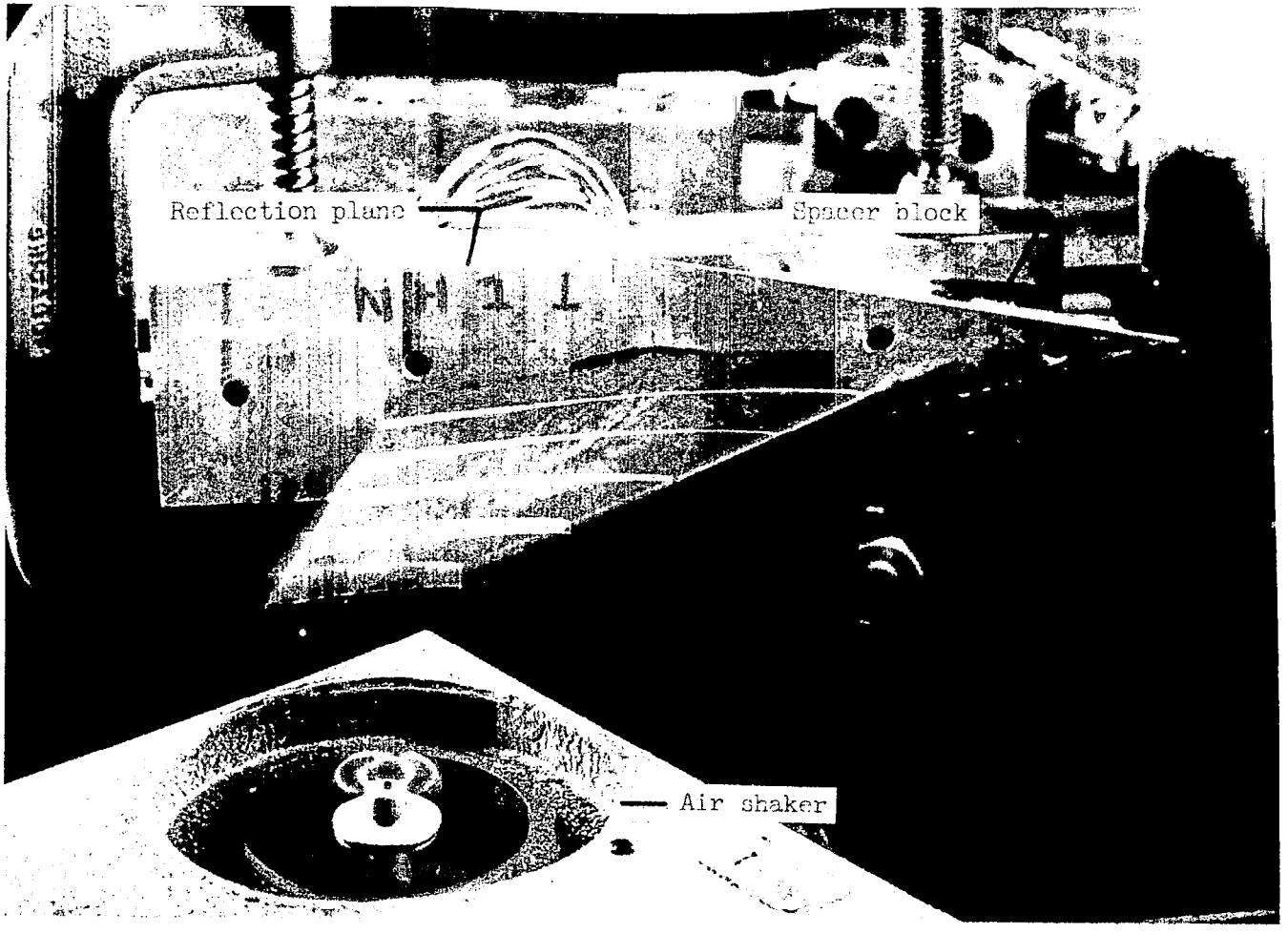


L-59-197

Figure 5.- Arrangement for determining modes and frequencies of model H-1. Model vibrating in the first mode.

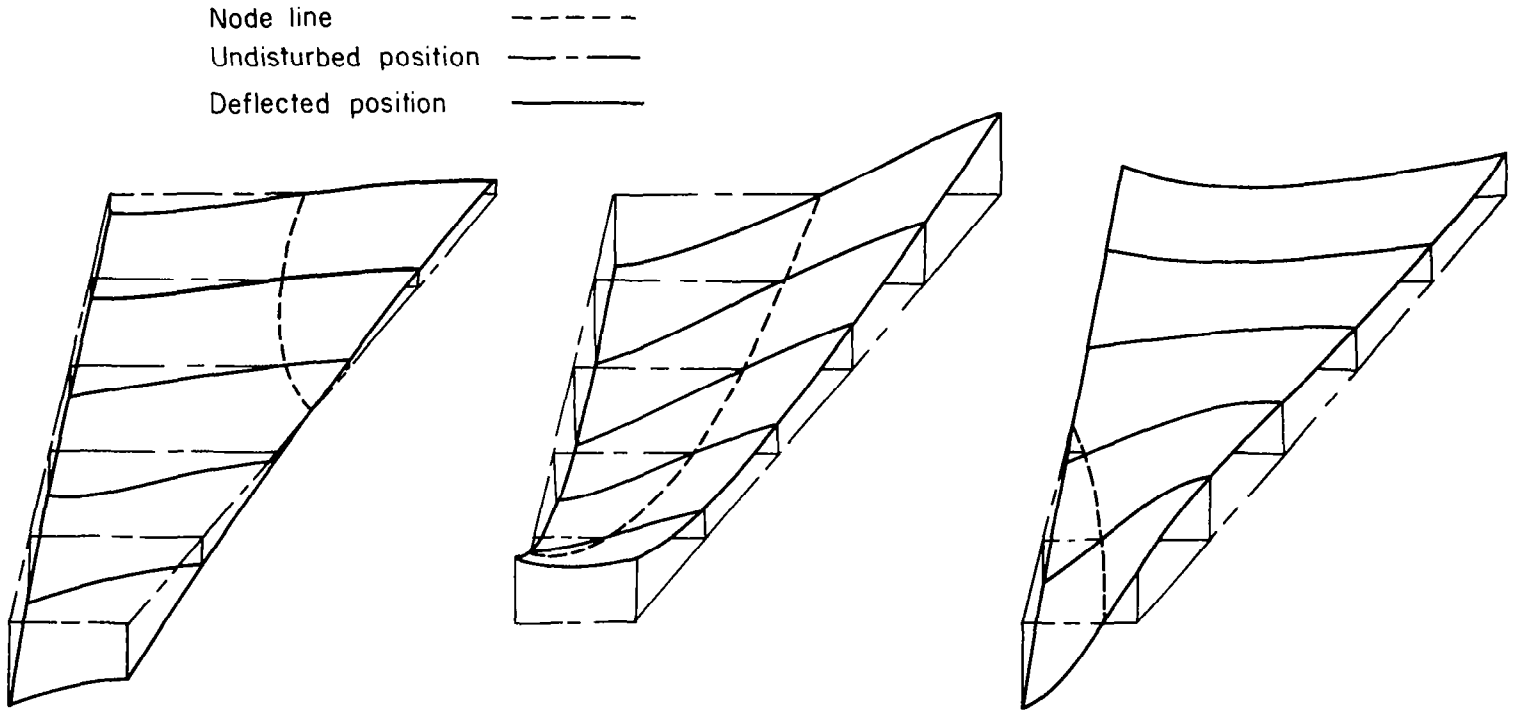


(a) First mode. (b) Second mode. (c) Third mode.

Figure 6.- Sketch of natural vibration modes of horizontal-tail model H-1.

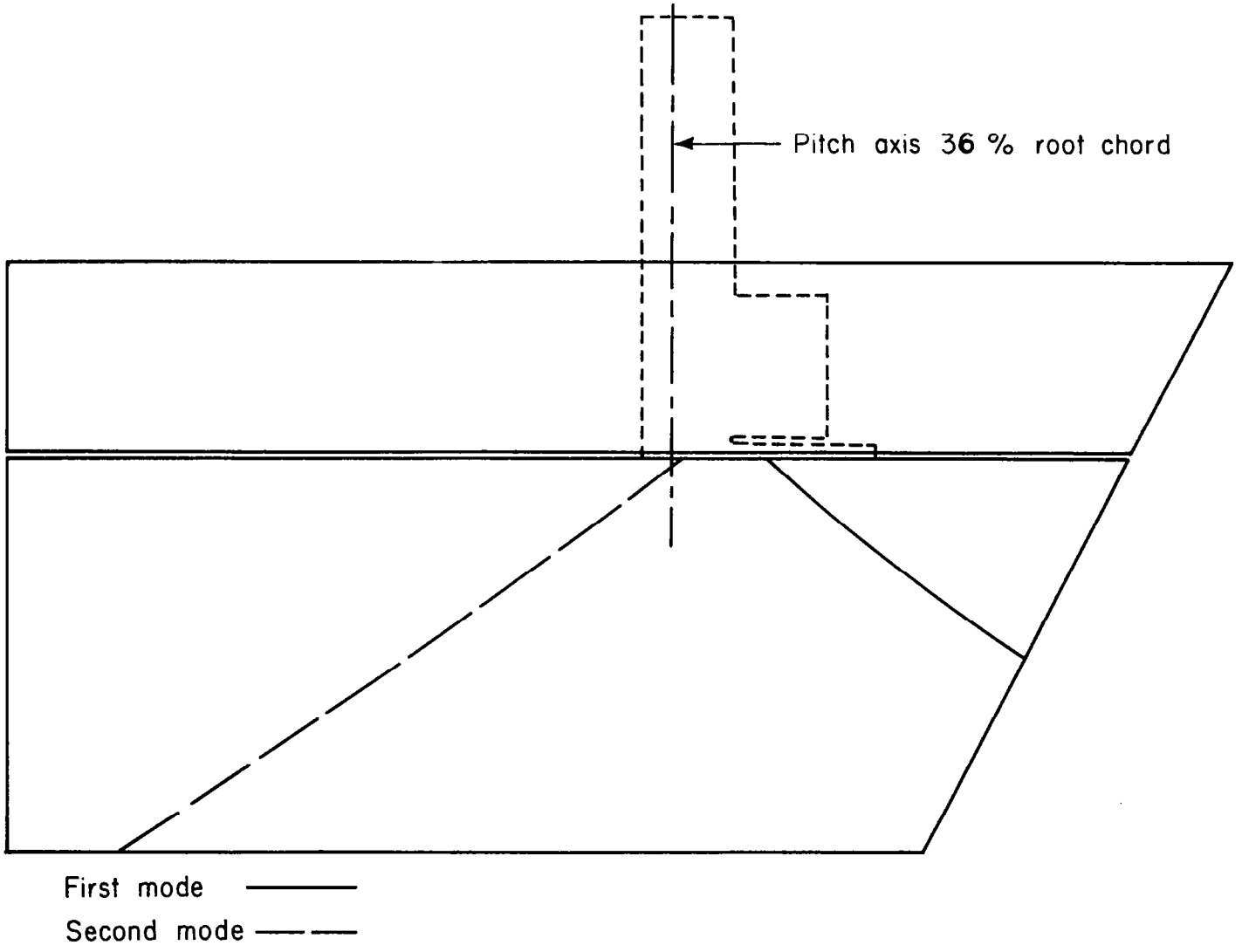


Figure 7.- Node lines of vertical-tail model V-1.

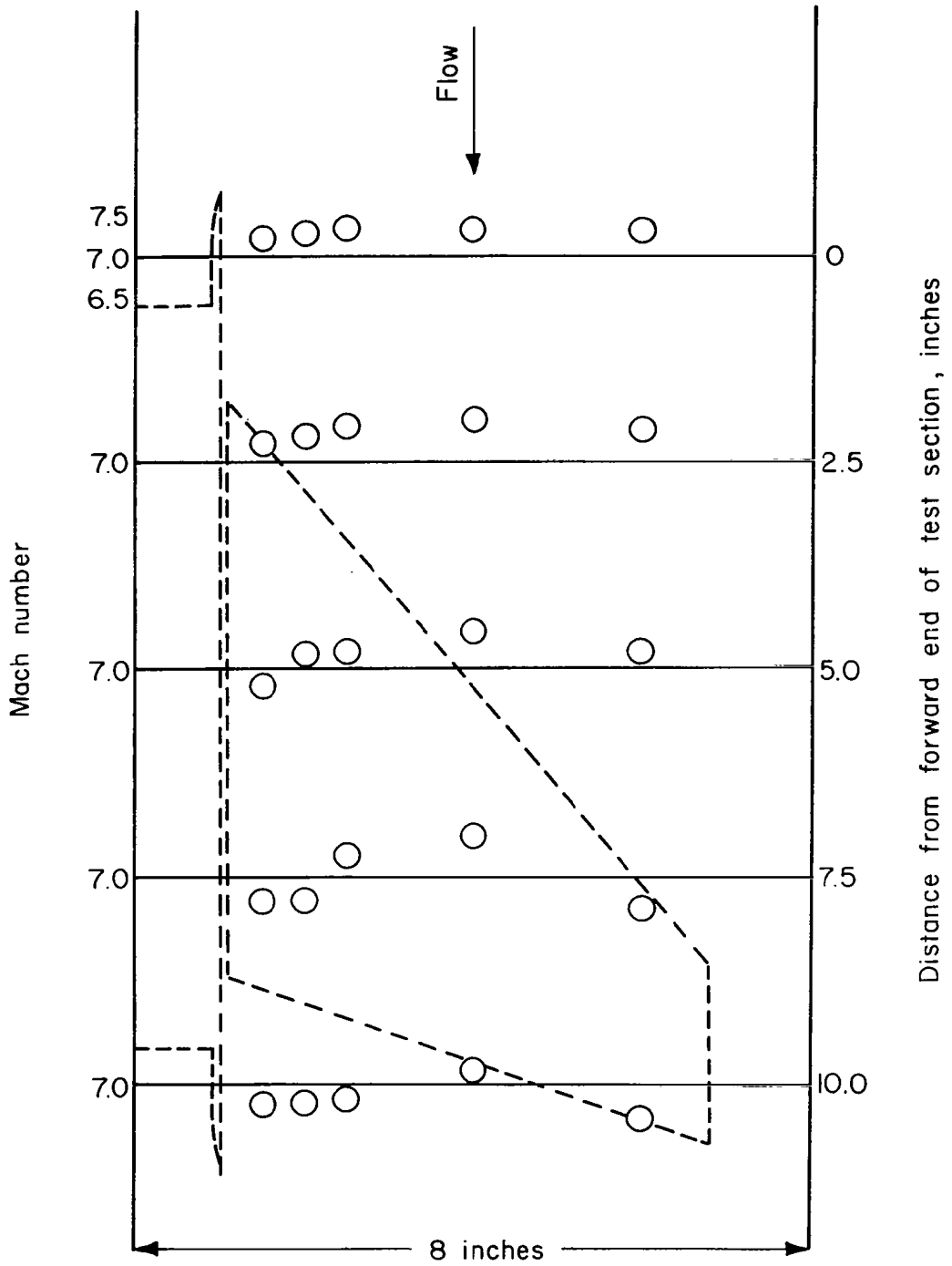


Figure 8.- Sketch showing Mach number distribution of five stations along the test section of the Langley 8-inch hypersonic aeroelasticity tunnel.

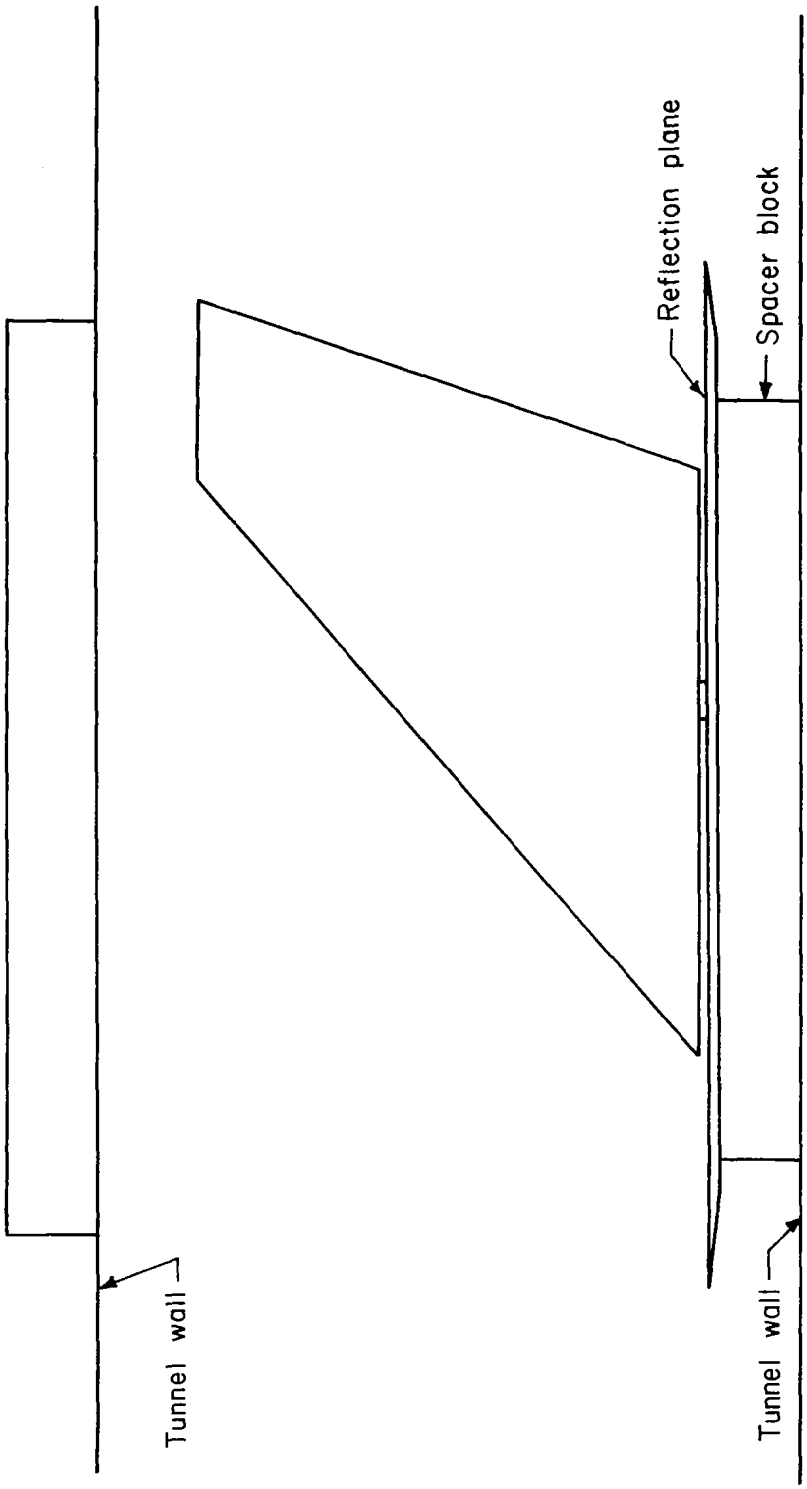


Figure 9.- Sketch of horizontal-tail model mounted in the tunnel.

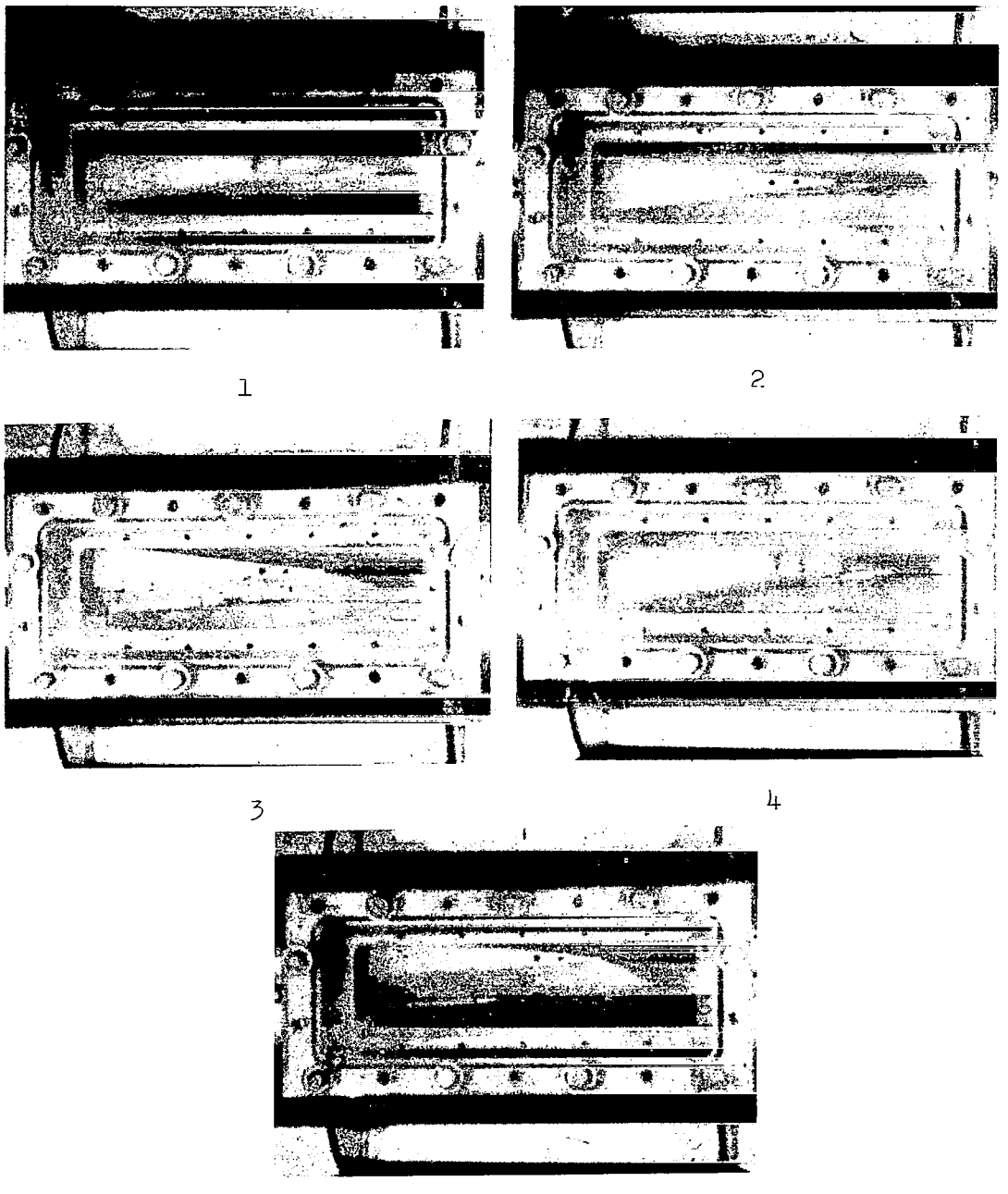


L-59-198

Figure 10.- Sequence of photographs showing flutter of the wedge-section control surface V-1.

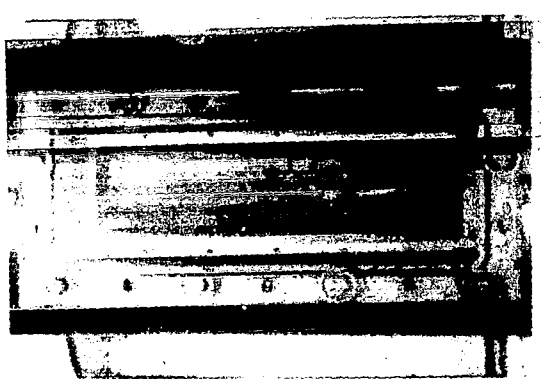

6

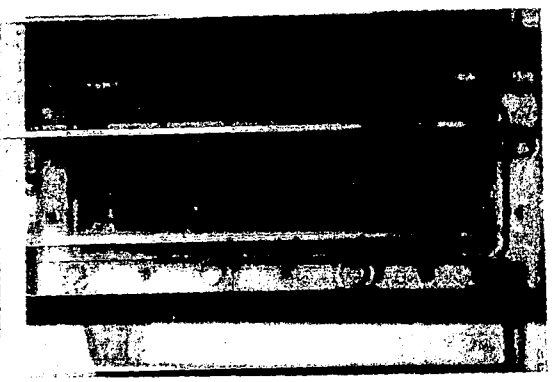

7

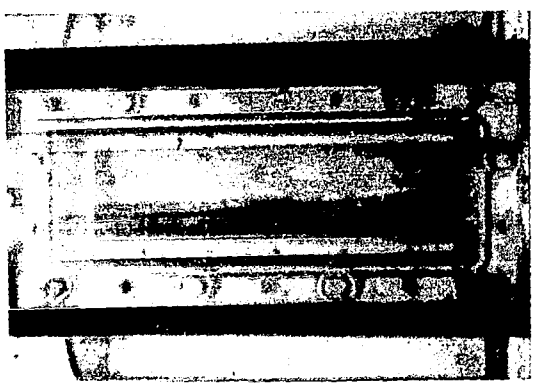

8

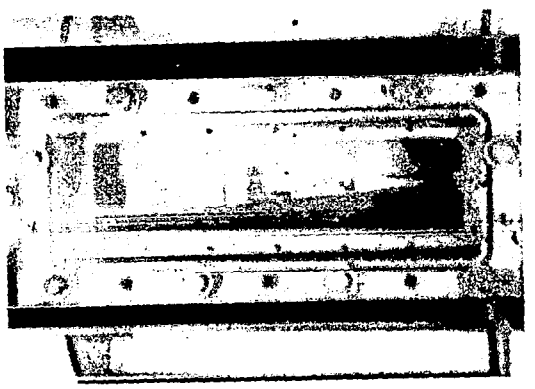

9

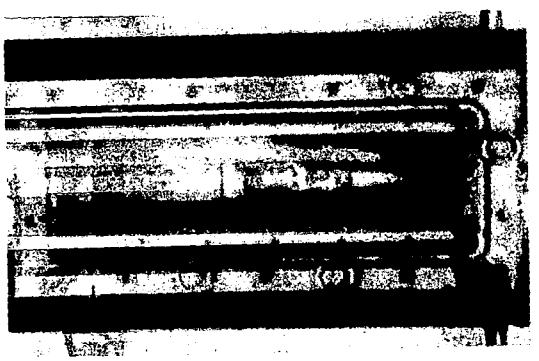

10

Figure 10.- Concluded. L-59-199

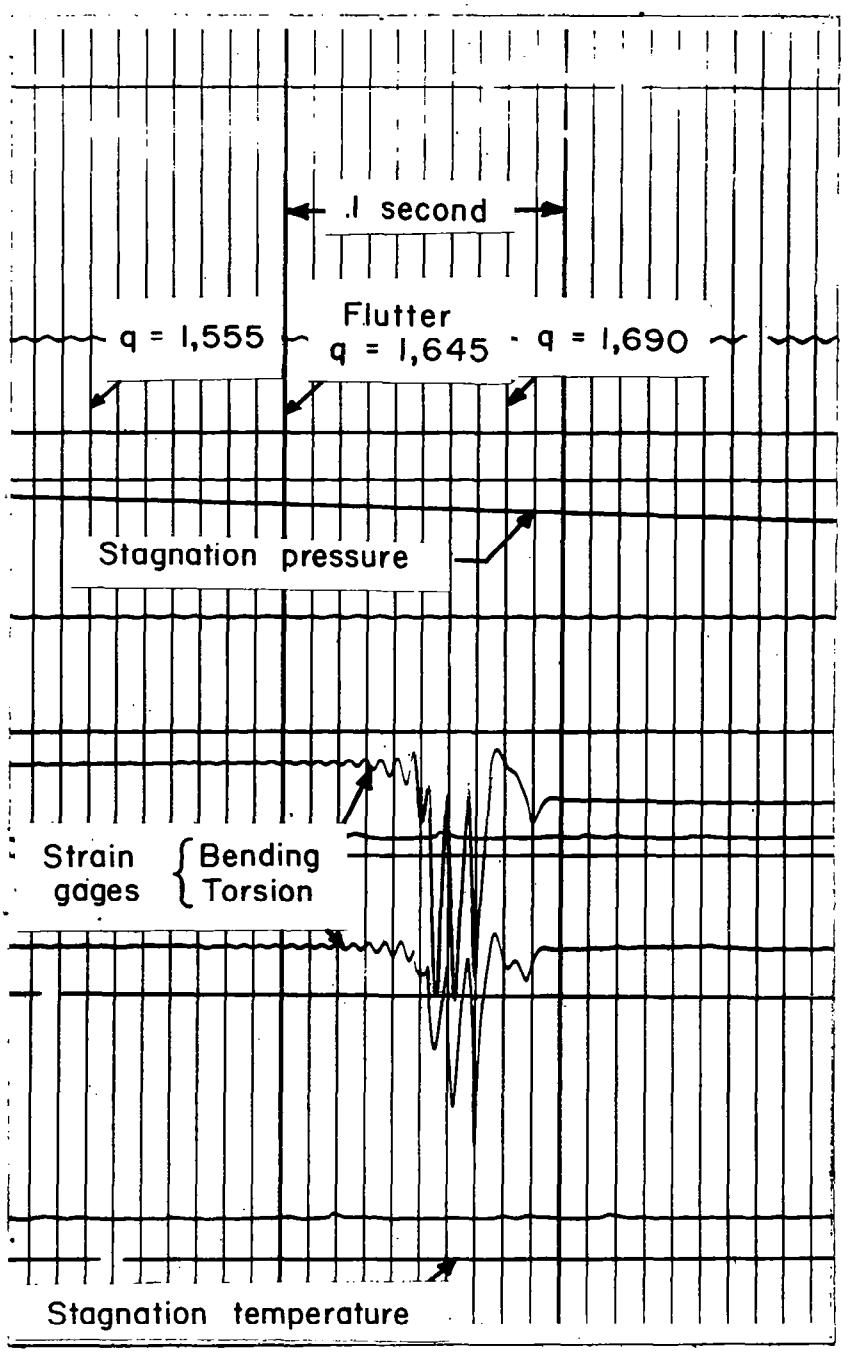


Figure 11.- Oscillograph record showing flutter of the vertical-tail model V-1. All unlabeled traces are idle channels.

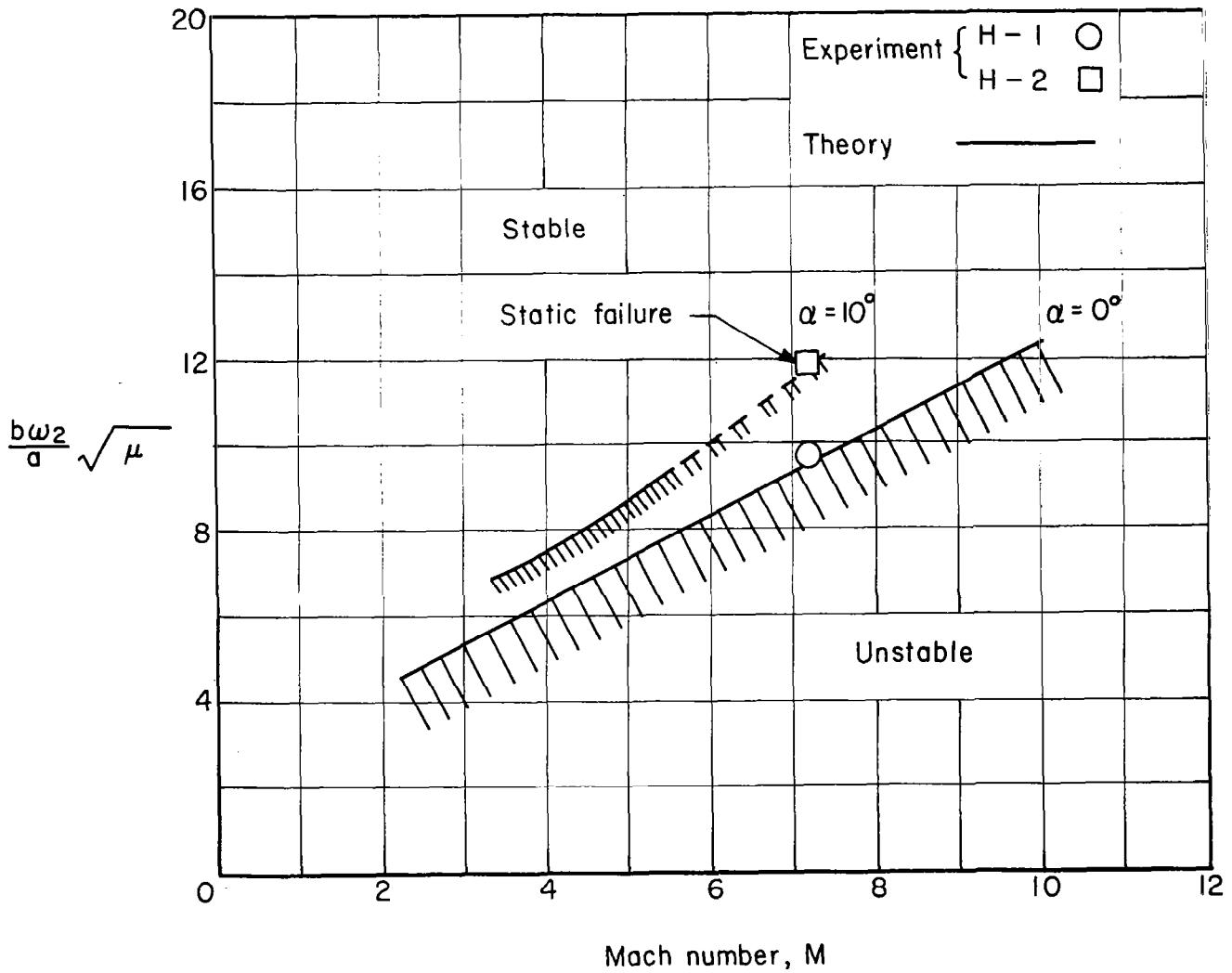


Figure 12.- Comparison of experimental results with theoretical flutter boundary for the horizontal-tail models.

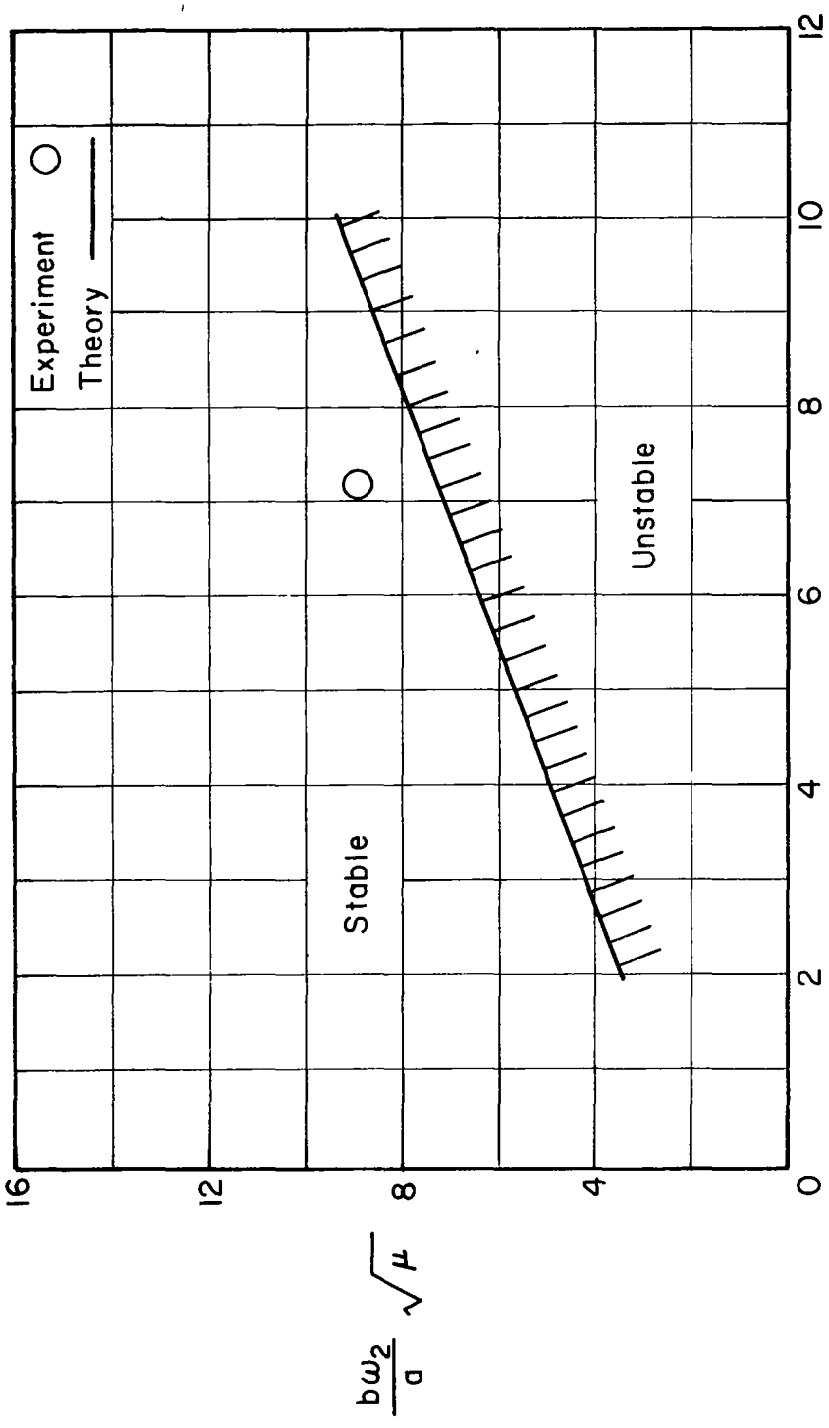


Figure 13.- Comparison of experimental result with theoretical flutter boundary for the vertical-tail model.